

International Journal of Modern Physics E
 © World Scientific Publishing Company

Study of Rotating High Energy Systems with the Differential HBT Method

L.P. Csernai

*Institute of Physics and Technology, University of Bergen, Allegaten 55, 5007 Bergen, Norway
 csernai@ift.uib.no*

S. Velle

*Institute of Physics and Technology, University of Bergen, Allegaten 55, 5007 Bergen, Norway
 sindre.velle@ift.uib.no*

Received Day Month Year
 Revised Day Month Year

Peripheral heavy ion reactions at ultra relativistic energies have large angular momentum that can be studied via two particle correlations using the Differential Hanbury Brown and Twiss method. In the present work we analyze the possibilities and sensitivity of the method in rotating, few source systems. Analytic results provide insight in the advantages of this method.

Keywords: Two particle correlation; Rotation; Heavy ion collisions.

PACS numbers: 25.75.Gz, 25.75.Nq

1. Introduction

Collective flow is one of the most dominant observable features in heavy ion reactions up to the highest available energies, and its global symmetries as well as its fluctuations are extensively studied. Especially at the highest energies for peripheral reaction the angular momentum of the initial state is substantial, which leads to observable rotation according to fluid dynamical estimates.¹ Furthermore the low viscosity quark-gluon fluid may lead to initial turbulent instabilities, like the Kelvin Helmholtz Instability (KHI), according to numerical fluid dynamical estimates,² which is also confirmed in a simplified analytic model.³ These turbulent phenomena further increase the rotation of the system, which also leads to a large vorticity and circulation of the participant zone one order of magnitude larger than from random fluctuations in the transverse plane.⁴⁻⁶ It is estimated² that the increased rotation can be observable via the increased v_1 -flow, but the v_1 signal at high energies is weak, so other observables of the rotation are also needed.

The two particle correlation method is used to determine the space-time size of the system emitting the observed particles, thus providing valuable information on

the exploding and expanding system at the freeze out stage of a heavy ion collision. This method is based on the Hanbury Brown and Twiss (HBT) method, originally used for the determination of the size of distant stars.^{7,8} In heavy ion collisions the HBT method was used first for the same purpose, the determination of the system size,⁹ but later also the ellipsoidal shape of the system and its tilt.^{10–13} It was also observed relatively early that the expansion of the system modifies the size estimates due to the collective radial flow velocity of the emitting system,¹⁴ while the effect of flow on two particle correlations was also analysed in great detail.¹⁵ Transport model studies have indicated that the HBT radius shows a minimum at the phase transition threshold.^{16,17}

Recently in AdS/CFT holography we have seen¹⁹ that the region of the phase diagram is dependent on the amount of angular momentum as well as instabilities in the plasma produced in these peripheral collisions. Whether the angular momentum is carried by rotation or by shear is of importance.

In heavy ion reactions the angular momentum is expected to generate local vorticity,⁴ which equilibrates with the internal angular momentum of the constituted particles and causes significant observable polarization after the final particle emission.²⁰

In Ref. 21 a method is used to do fluid dynamical model calculations and it was demonstrated that the introduced Differential HBT method can be used to measure the rotation of the system. We study this method hereby in simple and transparent few source fluid dynamical model with different symmetry structures. These type of models are frequently used to demonstrate different effect in a transparent way.^{22–25} These studies provide analytic results, show how we can detect rotation via two particle correlation functions, and what effects may cause difficulties in identifying rotation.

1.1. *The Emission Function*

The emission function and the hydrodynamical parametrization together with the Freeze Out (FO) layer have been studied²¹ earlier. The emission probability is proportional to $G(x)H(\tau)$:

$$S(x, \mathbf{p}) d^4x = p^\mu \hat{\sigma}_\mu(x) G(x) H(\tau) d\tau d^3x f(x, p) ,$$

where

$$H(\tau) = \frac{1}{(2\pi\Theta^2)^{1/2}} \exp \left[-\frac{(\tau - \bar{\tau})^2}{2\Theta^2} \right] , \quad (1)$$

and $G(x)$ is the ST emission density across the layer of the particles. For the phase space distribution we frequently use the Jüttner (relativistic Boltzmann) distribution, in terms of the local invariant scalar particle density the Jüttner distribution is²⁶

$$f^J(x, p) = \frac{n(x)}{C_n} \exp \left(-\frac{p^\mu u_\mu(x)}{T(x)} \right) , \quad (2)$$

where $C_n = 4\pi m^2 T K_2(m/T)$.

1.2. Pion Correlation Functions

The pion correlation function is defined as the inclusive two-particle distribution divided by the product of the inclusive one-particle distributions, such that:²⁷

$$C(p_1, p_2) = \frac{P_2(p_1, p_2)}{P_1(p_1)P_1(p_2)}, \quad (3)$$

where p_1 and p_2 are the 4-momenta of the pions and \mathbf{k} and \mathbf{q} are the average and relative momentum respectively.

We use a method for moving sources presented in Ref. 28. In the formulae the $\hbar = 1$ convention is used and k and q are considered as the wavenumber vectors. The correlation function is:

$$C(k, q) = 1 + \frac{R(k, q)}{\left| \int d^4x S(x, k) \right|^2}, \quad (4)$$

where

$$R(k, q) = \int d^4x_1 d^4x_2 \cos[q(x_1 - x_2)] S(x_1, k + q/2) S(x_2, k - q/2). \quad (5)$$

Here $R(k, q)$ can be calculated²⁸ via the function

$$J(k, q) = \int d^4x S(x, k + q/2) \exp(iqx) = \int d^4x S(x, k + q/2) [\cos(qx) + i \sin(qx)], \quad (6)$$

and we obtain the $R(k, q)$ function as

$$R(k, q) = \text{Re} [J(k, q) J(k, -q)] \quad (7)$$

Thus, the expression of the correlation function, Eq. (5) will be modified to

$$R(k, q) = \int d^4x_1 d^4x_2 S(x_1, k) S(x_2, k) \cos[q(x_1 - x_2)] \exp \left[-\frac{q}{2} \cdot \left(\frac{u(x_1)}{T(x_1)} - \frac{u(x_2)}{T(x_2)} \right) \right], \quad (8)$$

and the corresponding $J(k, q)$ function will become

$$J(k, q) = \int d^4x S(x, k) \exp \left[-\frac{q \cdot u(x)}{2T(x)} \right] \exp(iqx). \quad (9)$$

1.3. One Fluid Cell as Source

We now assume a source function, which is reduced to one Freeze Out (FO) time moment. Thus the integration over the 4-volume of an emission layer is reduced to the 3-volume of a FO hypersurface.²⁹ For simplicity, we assume FO along the timelike coordinate, t , where we assume a local Jüttner distribution. Thus, we have the source function as

$$S(x, k) = G(x) H(t) \exp \left(-\frac{k_\mu u^\mu(x)}{T(x)} \right) k^\mu \hat{\sigma}_\mu, \quad (10)$$

4 *L.P. Csernai, S. Velle*

where $k^\mu \hat{\sigma}_\mu$ is an invariant scalar and $\hat{\sigma}_\mu$ is the direction of emission unit vector,^{21,30} and for a single cell we use a simple quadratic parametrization for $n(x)$ as:

$$G(x) = \gamma n(x) = \gamma n_s \exp\left(-\frac{x^2 + y^2 + z^2}{2R^2}\right). \quad (11)$$

Here n_s is the average density of the Gaussian source, s , (or fluid cell) of mean radius R .

Single moving source: Let us take a single source which moves in the x -direction with a velocity v_x . Then we have, $u_s^\mu = \gamma_s(1, v_x, 0, 0)$, and the scalar product $k \cdot u_s/T_s = k_\mu u_s^\mu/T_s$ provides an additional contribution to the correlation function. However, in the case of a single fluid cell or a single source the velocity and the temperature do not change within the cell, so the modifying term in eq. (8) becomes unity. The source function becomes

$$S(x, k) = \frac{n(x) (k^\mu \hat{\sigma}_\mu)}{C_n} \exp\left[-\frac{k \cdot u_s}{T_s}\right], \quad (12)$$

where $[k \cdot u_s/T_s] = [\gamma_s(E_k - k_x v_x)/T_s]$ as used in Ref. 30, 21.

Within the single source (or fluid element) the velocity u_s and temperature T_s are assumed to be the same. The source or fluid element may have a density profile, but this profile should be the same for all cells (although the average density, n_s must not be the same. The spatial integrals can be performed in the rest frame of the cell, giving the same integral. In this simplest case we also assume that the FO direction is $\hat{\sigma}^\mu = (1, 0, 0, 0)$, so the τ -coordinate coincides with the t -coordinate, and it is orthogonal to the x, y, z -coordinates.

We can perform the integral along the t direction of $H(t)$, which gives unity and then the single particle distribution is

$$\begin{aligned} \int d^4x S(x, k) &= \frac{n_s (k^\mu \hat{\sigma}_\mu)}{C_n} \exp\left(-\frac{k \cdot u_s}{T_s}\right) \times \\ &\int_{-\infty}^{+\infty} H(t) dt \int_{-\infty}^{+\infty} e^{-\frac{x^2}{2R^2}} dx \int_{-\infty}^{+\infty} e^{-\frac{y^2}{2R^2}} dy \int_{-\infty}^{+\infty} e^{-\frac{z^2}{2R^2}} dz \\ &= n_s (k^\mu \hat{\sigma}_\mu) \exp\left(-\frac{k \cdot u_s}{T_s}\right) \frac{(2\pi R^2)^{3/2}}{C_n}, \end{aligned} \quad (13)$$

where T_s is the temperature of the source. The contribution to the nominator from Eq. (9) is

$$\begin{aligned} J(k, q) &= \int d^4x e^{iq \cdot x} e^{-q^0/(2T_s)} S(x, k) \exp\left[-\frac{q \cdot u_s}{2T_s}\right] = \\ &\frac{n_s (k^\mu \hat{\sigma}_\mu)}{C_n} (2\pi R^2)^{3/2} \exp\left[-\frac{k^0}{T_s}\right] \exp\left[-\frac{q^0}{2T_s}\right] \times \\ &\exp\left[-\frac{R^2}{2} q^2\right] \exp\left[-\frac{\Theta^2}{2} (\hat{\sigma}^\mu q_\mu)^2\right] \exp\left[-\frac{q \cdot u_s}{2T_s}\right], \end{aligned} \quad (14)$$

In the time integral the present choice of $\hat{\sigma}^\mu$ would give $(q^0)^2$, but we wanted to indicate that other choices are also possible and they would yield $(\hat{\sigma}^\mu q_\mu)^2$. In the $J(k, q)J(k, -q)$ product the terms $\exp[\pm q^0/(2T_s)]$ cancel each other. Also in the $J(k, q)J(k, -q)$ product the terms $\exp[\pm q \cdot u_s/(2T_s)]$ cancel each other, so the correlation function will not be dependent on the velocity in this case. Inserting these equations into (4) we get

$$C(k, q) = 1 + \exp\left(-(\Delta\tau)^2(\hat{\sigma}^\mu q_\mu)^2 - R^2 q^2\right). \quad (15)$$

If we have a source at a point in the FO layer, which is at a longer distance from the external side of the FO layer than Θ , then the contribution of the time integral from this point is reduced. In a few source model it is more transparent to describe this reduction by assigning a smaller weight factor to the contribution of the deeper lying source. See this in more detail in section 2.

If we tend to an infinitely narrow FO layer, $\Theta \rightarrow 0$, i.e. to a FO hypersurface, then

$$C(k, q) = 1 + \exp\left(-R^2 q^2\right). \quad (16)$$

The k dependence drops out from the correlation function, $C(k, q)$ as the k dependent parts are separable. The size of the fluid cells in a high resolution 3+1D fluid dynamical calculation is $(0.3\text{fm})^3$.²¹ With this resolution the *numerical viscosity* of the fluid dynamical calculation³¹ is the same as the estimated minimal viscosity of the QGP³² which occurs at the critical point of the phase transition.³³ Eq. (16) returns the standard correlation function for spherical source.

1.4. Two moving sources

For emission from two moving sources, two particle correlations were studied in Ref. 30. Here we use the present method. Now we assume that the two source system is symmetric both their positions are placed symmetrically and also their FO normal vectors, $\hat{\sigma}^\mu$, are the same (Fig. 1). If the normal were $\hat{\sigma}^\mu = (1, 0, 0, 0)$, then the invariant scalar $k^\mu \hat{\sigma}_\mu$ would be $k^0 = E_k$, although we do not need this additional requirement to illustrate the correlation function, which would arise from an idealized symmetric system. We also assume that the time distributions, $H(\tau)$ for the two sources are identical, so these can be integrated simultaneously and yield unity. We now have two sources moving in opposite directions, so that $u_s = u_1$ or u_2 where $u_1^\mu = (\gamma_s, \gamma_s \mathbf{v}_1)$, $u_2^\mu = \bar{u}_s^\mu = (\gamma_s, \gamma_s (-\mathbf{v}_1))$, and $\mathbf{u}_s \equiv \gamma_s \mathbf{v}_s$, so that $\mathbf{u}_1 = -\mathbf{u}_2$, see Fig. 1. Similarly, $x_s = x_1$ or x_2 where $x_s^\mu = (t_s, \mathbf{x}_s)$, $\bar{x}_s^\mu = (t_s, -\mathbf{x}_s)$, and $\mathbf{x}_1 = -\mathbf{x}_2$. For now we also assume that FO happens at a $t = \text{const.}$ FO hypersurface, so $d\hat{\sigma}^\mu = (1, 0, 0, 0)$ and so $t_1 = t_2$.

If we have several sources then the source function in Jüttner approximation is

$$S(x, k) = \sum_s S_s(x, k) = (k^\mu \hat{\sigma}_\mu) \sum_s \frac{n_s(x)}{C_{ns}} \exp\left[-\frac{k \cdot u_s}{T_s}\right], \quad (17)$$

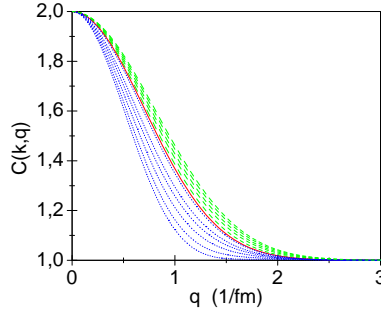


Fig. 1. (color online) Two moving sources in the reaction ($[x - z]$) plane with a distance between them of $2d$ in the z -direction. The sources are moving in the directions indicated by the (red) arrows.

while the J function is

$$J(k, q) = \sum_s \exp \left[-\frac{q \cdot u_s}{2T_s} \right] \exp(iqx_s) \int_S d^3x S_s(x, k) \exp(iqx), \quad (18)$$

where x_s is the 4-position of the center of source s , and the spatial integrals run separately for each of the identical sources, i.e. we assume fluid cells with identical density profiles, but with different densities, n_s , velocities, u_s and temperatures, T_s .

The spatial integral for one source is the same as for a single source. Thus,

$$\begin{aligned} \int d^3x S(x, k) &= \sum_s \int_S d^3x S_s(x, k) = \\ &= (k^\mu \hat{\sigma}_\mu) (2\pi R^2)^{3/2} \frac{n_s}{C_{ns}} \exp \left(-\frac{k^0 \gamma_s}{T_s} \right) \left[\exp \left(\frac{\mathbf{k} \cdot \mathbf{u}_s}{T_s} \right) + \exp \left(-\frac{\mathbf{k} \cdot \mathbf{u}_s}{T_s} \right) \right]. \end{aligned} \quad (19)$$

The function $J(k, q)$ becomes

$$\begin{aligned} J(k, q) &= \sum_s \exp \left[-\frac{q \cdot u_s}{2T_s} \right] \exp(iqx_s) \int_S d^4x S_s(x, k) \exp(iqx) = \\ &= (k^\mu \hat{\sigma}_\mu) (2\pi R^2)^{3/2} \exp \left(-\frac{R^2 q^2}{2} \right) \sum_s \frac{n_s}{C_{ns}} \exp \left[-\frac{\mathbf{k} \cdot \mathbf{u}_s}{T_s} \right] \exp \left[-\frac{q \cdot u_s}{2T_s} \right] \exp(iqx_s) = \\ &= (k^\mu \hat{\sigma}_\mu) (2\pi R^2)^{3/2} \exp \left(-\frac{R^2 q^2}{2} \right) \frac{n_s}{C_{ns}} \exp \left[-\frac{k^0 \gamma_s}{T_s} \right] \exp \left[-\frac{q^0 \gamma_s}{2 T_s} \right] \exp(iq^0 x_s^0) \times \\ &\quad \left[\exp \left[\frac{\mathbf{k} \cdot \mathbf{u}_s}{T_s} \right] \exp \left[\frac{\mathbf{q} \cdot \mathbf{u}_s}{2T_s} \right] \exp(-i\mathbf{q} \cdot \mathbf{x}_s) + \exp \left[-\frac{\mathbf{k} \cdot \mathbf{u}_s}{T_s} \right] \exp \left[-\frac{\mathbf{q} \cdot \mathbf{u}_s}{2T_s} \right] \exp(i\mathbf{q} \cdot \mathbf{x}_s) \right], \end{aligned} \quad (20)$$

where the factor $\exp(iq^0 x_s^0)$ can be dropped if the FO time distribution is simultaneous for the two sources, because then $x_s^0 = 0$. Consequently, if the two sources

have the same parameters, just opposite locations with respect to the center, and opposite velocities, then the correlation function from Eq. (4) is

$$C(k, q) = 1 + \exp(-R^2 q^2) \frac{\cosh\left(\frac{2\mathbf{k}\mathbf{u}_s}{T_s}\right) + \cosh\left(\frac{\mathbf{q}\mathbf{u}_s}{T_s}\right) \cos(2\mathbf{q}\mathbf{x}_s)}{\cosh\left(\frac{2\mathbf{k}\mathbf{u}_s}{T_s}\right) + 1}. \quad (21)$$

If the velocity of the two sources vanishes this results returns the expression for two static sources obtained in Ref. 30.

If we have two sources placed at $x = \pm d_z$, and with the velocity in the $\pm x$ -direction, $\pm v_x$, then the correlation function for the k_x direction becomes:

$$\begin{aligned} C(k_x, q_x) &= 1 + \exp(-R^2 q_x^2) \frac{\cosh\left(\frac{2\gamma k_x v_x}{T_s}\right) + \cosh\left(\frac{\gamma q_x v_x}{T_s}\right)}{\cosh\left(\frac{2\gamma k_x v_x}{T_s}\right) + 1}, \\ C(k_x, q_y) &= 1 + \exp(-R^2 q_y^2), \\ C(k_x, q_z) &= 1 + \exp(-R^2 q_z^2) \frac{\cosh\left(\frac{2\gamma k_x v_x}{T_s}\right) + \cos(2q_z d_z)}{\cosh\left(\frac{2\gamma k_x v_x}{T_s}\right) + 1}. \end{aligned} \quad (22)$$

Other equations for sources in different locations or the correlation function for k_y and k_z can be found using Eq. (21). The correlation function for different source

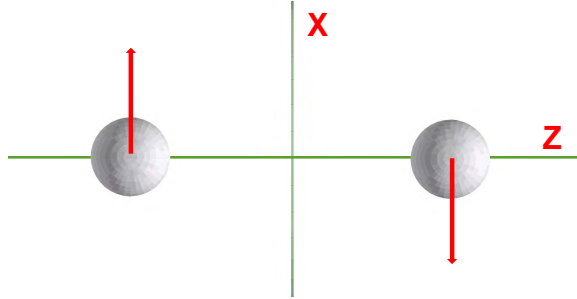


Fig. 2. (color online) The correlation functions, $C(k, q)$ for two moving sources where the displacement of the sources is in the z -direction, and the center-of-mass momentum, \mathbf{k} , of emitted particles is in the x -direction. The *dashed green lines* are for the relative momentum, q_z , the *solid red line* is for q_y and *dotted blue lines* are for q_x . For large values of the center-of-mass momentum k_x the correlation functions $C(k_x, q_x)$ and $C(k_x, q_z)$ will approach the correlation function $C(k_x, q_y)$ (red line). For q_x (blue lines) the displacements are $d_x = 1, 0$ fm, and for q_z (green lines) the velocity is chosen such that $\gamma v_z/T_s = 1.0$ fm. The values of k_z are for the blue lines: 0.25, 0.5, 0.75, 1.0, 1.25 and 2.0 fm⁻¹ and for the green lines: 0.25, 0.5, 0.75, 1.0 and 1.5 fm⁻¹.

locations and velocities are similar. The cosine term appears in the same direction as the axis at which the sources are located and the hyperbolic cosine in the direction of the velocity. The distribution does depend on the magnitude of the flow velocity, v_x , but not on its direction! This arises from the fact that the detectors are **assumed to be** reached from both sides of the system with opposite velocities

with equal probability. Unfortunately the dominant direction of flow (see Fig. 3) is the beam direction (z -direction), where we have no possibility to place high acceptance detectors. At the same time the strongest effect of the flow appears in this direction.

In the case of Fig. 2 the flow has the most dominant effect in the k_x -direction, which is accessible for detection. The x -directed flow, however, is more sensitively dependent on secondary effects, like the Kelvin-Helmholtz Instability.²

In this configuration of the sources the magnitude of the flow velocity makes visible change in $C(k, q)$, in the (k_x, q_x) -direction also, which is detectable by the usual detector configurations. Still the direction of the rotation does not appear in the observables, eq. (21), with the approach presented here.

For these two-particle correlation measurements it is necessary to identify independently, event by event the global collective reaction plane azimuth, Ψ_{RP} , experimentally and the corresponding event by event center of mass of the system (e.g. with the method in Ref. 22, 23). Knowing these we can identify the k_x -direction (and the k_y -direction also).

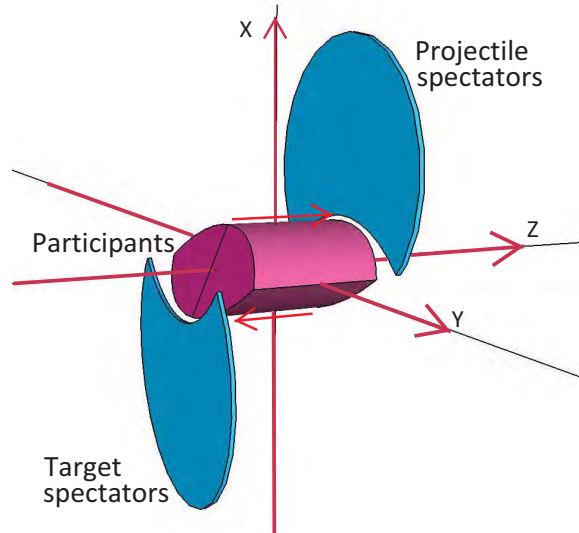


Fig. 3. (Color online) Typical orientation of the spatial axes in case of an ultra-relativistic heavy ion reaction shortly after the impact. In the configuration space the projectile and target appear to be flat due to the Lorentz contraction.

It is important to mention that to detect rotation the accurate identification of the reaction plane and its proper orientation is necessary. Furthermore, not only the reaction plane with proper direction but also the event by event center of mass (c.m.) should be identified.^{22,23} This hardly ever done! In both cases the use of zero

degree calorimeters provide an adequate tool as these are sensitive to the spectator residues.

1.5. Four Fluid Cell Sources

Four sources can be treated as a combination of two moving double source systems. We use the same parameters as under paragraph 1.4, where s_1 and s_2 will be the two different pairs of sources with different locations and velocities. See Fig. 4.

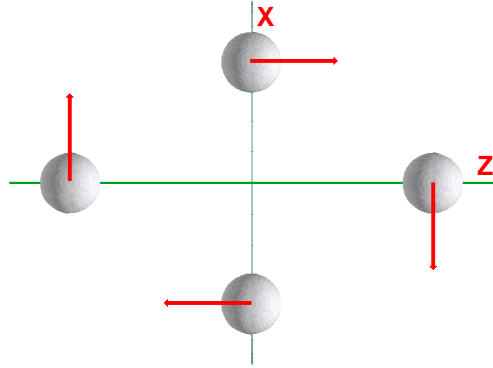


Fig. 4. (color online) Four moving sources in the reaction $([x-z])$ plane, one pair, s_1 , is separated in the x - directions and the other, s_2 , is in the z - direction. The sources are moving in the directions indicated by the (red) arrows, $\pm \mathbf{u}_{s1}$ for the 1st pair and $\pm \mathbf{u}_{s2}$ for the other.

So we obtain the correlation function for four sources as:

$$\begin{aligned}
 C(k, q) = & \exp(-R^2 q^2) \times \\
 & \left[\cosh\left(\frac{2\mathbf{k} \cdot \mathbf{u}_{s1}}{T_s}\right) + \cosh\left(\frac{\mathbf{q} \cdot \mathbf{u}_{s1}}{T_s}\right) \cos(2\mathbf{q} \cdot \mathbf{x}_{s1}) + \right. \\
 & \cosh\left(\frac{2\mathbf{k} \cdot \mathbf{u}_{s2}}{T_s}\right) \cosh\left(\frac{\mathbf{q} \cdot \mathbf{u}_{s2}}{T_s}\right) \cos(2\mathbf{q} \cdot \mathbf{x}_{s2}) + \\
 & 2 \cosh\left(\frac{\mathbf{k} \cdot (\mathbf{u}_{s1} - \mathbf{u}_{s2})}{T_s}\right) \cosh\left(\frac{\mathbf{q} \cdot (\mathbf{u}_{s1} + \mathbf{u}_{s2})}{2T_s}\right) \cos(\mathbf{q} \cdot (\mathbf{x}_{s1} + \mathbf{x}_{s2})) + \\
 & \left. 2 \cosh\left(\frac{\mathbf{k} \cdot (\mathbf{u}_{s1} + \mathbf{u}_{s2})}{T_s}\right) \cosh\left(\frac{\mathbf{q} \cdot (\mathbf{u}_{s1} - \mathbf{u}_{s2})}{2T_s}\right) \cos(\mathbf{q} \cdot (\mathbf{x}_{s1} - \mathbf{x}_{s2})) \right] \times \\
 & \left[\cosh\left(\frac{2\mathbf{k} \cdot \mathbf{u}_{s1}}{T_s}\right) + \cosh\left(\frac{2\mathbf{k} \cdot \mathbf{u}_{s2}}{T_s}\right) + 2 \cosh\left(\frac{\mathbf{k} \cdot (\mathbf{u}_{s1} + \mathbf{u}_{s2})}{T_s}\right) + \right. \\
 & \left. 2 \cosh\left(\frac{\mathbf{k} \cdot (\mathbf{u}_{s1} - \mathbf{u}_{s2})}{T_s}\right) + 2 \right]^{-1}.
 \end{aligned} \tag{23}$$

If $s_1 = s_2$ then we recover Eq. (21).

In the case of a rotating but symmetric system the displacements and velocities are of equal magnitude and are orthogonal to each other in the two pairs: $\mathbf{x}_{s_1} \perp \mathbf{x}_{s_2}$ and $\mathbf{u}_{s_1} \perp \mathbf{u}_{s_2}$. Thus a simple sign change of the velocity for one of the pairs or both does not change the result, and so the rotation can be identified, but this evaluation does not provide sensitivity to the direction of the rotation. The reason is in the over-simplified freeze out assumption as we mentioned already at the end of paragraph 1.4.

Four Sources with Flow Circulation: Recent fluid dynamical studies indicate,^{1,2} that due to the initial shear and angular momentum the early fluid dynamical development has significant flow vorticity and circulation on the reaction plane. These were recently evaluated.⁴ At the present LHC Pb+Pb collision energy in the mentioned fluid dynamical model calculation the maximum value of vorticity, ω , was found exceeding 3 c/fm, and the circulation after 6 fm/c flow development and expansion was still around 4-5 fm·c. This vorticity in the reaction plane was more than an order of magnitude bigger than in the transverse plane estimated from random fluctuations.^{5,6}

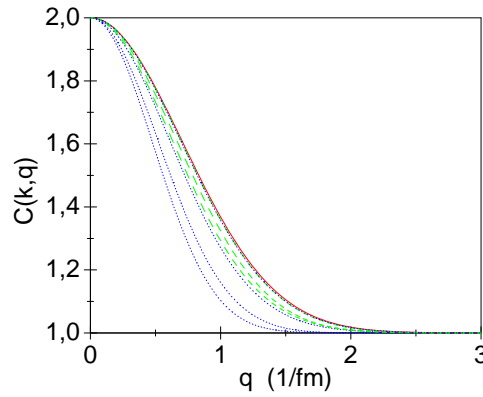


Fig. 5. (color online) The correlation functions, $C(k, q)$, for 4 sources where the displacement is such that there is one source pair on the x-axis and one the z-axis, the center-of-mass momentum of the emitted particles, \mathbf{k} , is in the x-direction. The *dotted blue lines* are for the velocity $v = 0.5c$ and displacement $d_x = d_z = 1.6$ fm. The *dashed green lines* are for the velocity $v = 0.8c$ and displacement $d_x = d_z = 1.0$ fm. $T_s = 0.20$ GeV. In both cases the circulation is $\Gamma = 5$ fm·c. The values of k_x are for the *blue lines*: 0.5, 1.5, 3.0 and 6.0 fm⁻¹ and for the *green lines*: 0.5, 1.5 and 3.0 fm⁻¹. The *solid red line* is the correlation function $C(k_x, q_y)$. For large values of the center-of-mass momentum k_x the correlation functions $C(k_x, q_x)$ and $C(k_x, q_z)$ will approach the correlation function $C(k_x, q_y)$. The larger displacement and smaller rotation velocity leads to stronger deviation from the unaffected correlation function $C(k_x, q_y)$.

In this section we will look at the four source correlation function with similar circulation as in the above mentioned fluid dynamical model estimates in the reaction plane.²¹ See Fig. 4. We will simulate a circulation value $\Gamma = 5 \text{ fm} \cdot c$. We

use Eq. (23) where the center-of-mass momentum, \mathbf{k} points in the x – direction. Since the position and velocity are of the same value and because of symmetry the correlation functions $C(k_x, q_x)$ and $C(k_x, q_z)$ provide the same values. So we take the correlation function $C(k_x, q_x)$ and we have afterwards some simplifications. See Fig. 5.

$$C(k_x, q_x) = 1 + \exp(-R^2 q^2) \left[1 + \cos(2q_x d) + \cosh\left(2 \frac{k_x \gamma v_x}{T_s}\right) + \cosh\left(\frac{q_x \gamma v_x}{T_s}\right) + 4 \cosh\left(\frac{k_x \gamma v_x}{T_s}\right) \cosh\left(\frac{q_x \gamma v_x}{2T_s}\right) \cos(q_x d) \right] \left[\cosh\left(\frac{2k_x \gamma v_x}{T_s}\right) + 4 \cosh\left(\frac{k_x \gamma v_x}{T_s}\right) + 3 \right]^{-1} \quad (24)$$

For $C(k_x, q_y)$ we have the same result as we had for the two moving sources. Here

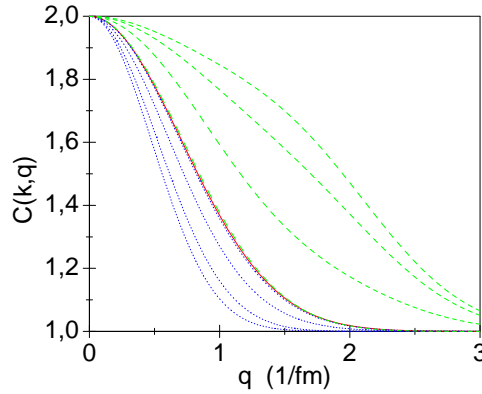


Fig. 6. (color online) The correlation functions, $C(k, q)$, for 4 sources where the displacement is such that there is one source pair on the x -axis and one the z -axis, the center-of-mass momentum of the emitted particles, \mathbf{k} , is in the x -direction. The *dotted blue lines* are for the velocity $v = 0.5c$ and displacement $d_x = d_z = 1.6$ fm (same as in the previous figure). The *dashed green lines* are for the velocity $v = 0.95c$ and displacement $d_x = d_z = 0.84$ fm, $T_s = 0.20$ GeV. The values of k_x are: for the *blue lines* 0.5, 1.5, 3.0 and 6.0 fm^{-1} and for the *green lines* 0.1, 0.25, 0.5 and 1.5 fm^{-1} . The *solid red line* is the correlation function $C(k_x, q_y)$. For large values of the center-of-mass momentum k_x the correlation functions $C(k_x, q_x)$ and $C(k_x, q_z)$ will approach the correlation function $C(k_x, q_y)$. Now for the dashed green lines with even higher velocity and smaller displacement, the deviation is significant and it is in the positive direction.

the flow and displacement have no effect. See Fig. 6.

Let us look at comparisons for similar circulations and for similar displacements. We see that an increase in the displacement of the sources gives a increase in the apparent size of the system (narrower q -distribution). We also see that the measured size of the system increases with decreasing velocity. At the same time the shape of correlation functions are becoming less and less Gaussian as the flow velocities increase. At the same time the structure of the correlation function is also

very different in different directions, which is not the case for spherical or linear expansion. This indicates that the rotating system contributes to essential non-Gaussian modifications, which can be seen directly in the correlation function, but they would become invisible if we would like to fit these data with a set of Gaussians. Earlier works studied the correlation function at different angles or pseudorapidities with Gaussian parametrizations,^{10,15} however, for rotating systems this is not the most sensitive way of presenting the results.

2. Asymmetric Sources

We have seen in the previous few source model examples that a highly symmetric source may result in correlation functions that are sensitive to rotation, however, these results were not sensitive to the direction of the rotation, which seems to be unrealistic. We saw that this result is a consequence of the assumption that both of the members of a symmetric pair contribute equally to the correlation function even if one is at the side of the system facing the detector and the other is on the opposite side. The expansion velocities are also opposite at the opposite sides. The dense and hot nuclear matter or the Quark-gluon Plasma are strongly interacting, and for the most of the observed particle types the detection of a particle from the side of the system, – which is not facing the detector but points to the opposite direction, – is significantly less probable. The reason is partly in the diverging velocities during the expansion and partly to the lower emission probability from earlier (deeper) layers of the source from the external edge of the timelike (or spacelike) FO layer. This feature is recognized for a long time and discussed in detail by now. This topic has an extended literature, and this feature destructs the symmetry of emission of from source pairs at the opposite sides of the system.^{15,29,34–48}

For the study of realistic systems where the emission is dominated by the side of the system, which is facing the detector, we cannot use the assumption of the symmetry among pairs or groups of the sources from opposite sides of the system. Even if the FO layer has a time-like normal direction, $\hat{\sigma}^\mu$ the $(k^\mu \hat{\sigma}^\mu)$ factor yields a substantial emission difference between the opposite sides of the system. This simple freeze-out emission probability factor was later taken into account in earlier theoretical two particle correlation studies, see e.g. Ref. 21 and Ref. 30.

2.1. The Emission Probability

It was first recognized that the freeze out with the Cooper-Fry description,²⁹ may lead to negative contributions for particles, which move towards the center of the system and not in the direction out, towards the detectors. The first proposal to remedy this problem came from Bugaev,⁴⁰ which led to the introduction of an improved post freeze out distribution in the Cooper-Frye description, first with the Cut-Jüttner distribution^{40,42} and then by the Cancelling-Jüttner distribution.⁴⁶

Later the necessity to introduce an escape probability, P_{esc} was pointed out. The escape probability was then introduced and analysed in a series of publications,^{34–36,48} in transport theoretical approaches. It was pointed out that even if

the pre FO distribution is a locally equilibrated isotropic distribution, the freeze out process and the escape probability will provide a nonisotropic distribution.

The escape probability introduced in the works,^{34–36,48} for a space-time surface layer of the system of thickness L , pointing in the four direction $\hat{\sigma}^\mu$ was given at a point x^μ inside the freeze out layer as

$$P_{esc}(x) \propto \left(\frac{L}{L - x^\mu \hat{\sigma}_\mu} \right) \left(\frac{p^\mu \hat{\sigma}_\mu}{p^\mu u_\mu} \right) \Theta(p^\mu \hat{\sigma}_\mu), \quad (25)$$

where p^μ is the momentum of the escaping particle, $u^\mu(x)$ is the local flow velocity and $s = x^\mu \hat{\sigma}_\mu$ is the distance of the emission point from the inside boundary of the layer. The first multiplicative term describes higher emission probability to the particles, which are emitted closer to the outside boundary of the layer, the second multiplicative term describes the higher emission probability for the particles, which move in the normal direction of the surface, because these should cross less material in the layer. The last term secures that only those particles can escape, which move outwards through the layer.

The correlation function, $C(k, q)$ is always measured in a given direction of the detector, \mathbf{k} . Obviously only those particles can reach the detector, which satisfy $k^\mu \hat{\sigma}_\mu > 0$. Thus in the calculation of $C(k, q)$ for a given $\hat{\mathbf{k}}$ -direction we can exclude the parts of the freeze out layer where $k^\mu \hat{\sigma}_\mu < 0$ (see Eq. (10) of Ref. 15 or Ref. 40). For time-like FO a simplest approximation for the emission possibility is $P_{esc}(x) \propto k^\mu u_\mu(x)$.³⁰

2.2. Emission probabilities for few sources

Two sources:

In the configuration where two sources are in the beam-, z -direction, the observation can be in different $\hat{\mathbf{k}}$ -directions. If $\hat{\mathbf{k}}$ points into the $\pm y$ -direction, then the probabilities must be identical so emission probabilities do not lead to any change.

If $\hat{\mathbf{k}}$ points into the $\pm x$ -direction, then one of the sources is closer to the detector and may shadow the more distant one. Thus, we can just introduce two positive weight factors so that w_c is the weight for the cells closer to the detector and w_s is for the cells which are far from the detector measuring the average momentum \mathbf{k} . These weights are the same for the calculation of the nominator and denominator of the correlation function, so their normalization does not influence the correlation function.

As not all emitted particles reach a given detector the normalization is also dependent on the direction of the detector. Thus, we evaluate the correlation function this way. This immediately changes the earlier result (22), because it breaks the symmetry between the two sources. We can simply repeat the calculation for two moving sources in section 1.4, modifying the derivation of Eq. (21) and obtain the

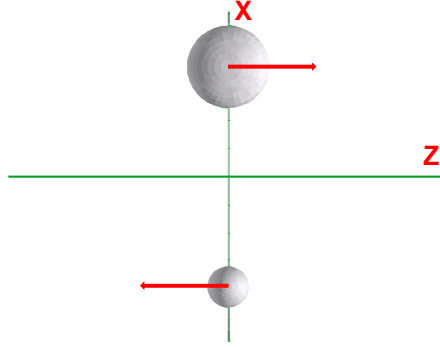


Fig. 7. (color online) Two moving sources in the reaction ($[x-z]$) plane, separated in the x -direction (case (ii) in the text). The sources are moving in the directions indicated by the (red) arrows. The detector is in the positive x -direction, thus the source on this side has more dominant emission into this direction, and this is indicated by the bigger size of the source on this side.

general result

$$C(k, q) \Big|_{+x} = 1 + \exp(-R^2 q^2) \times \frac{w_c^2 e^{\frac{2\mathbf{k}\mathbf{u}_s}{T_s}} + w_s^2 e^{-\frac{2\mathbf{k}\mathbf{u}_s}{T_s}} + 2w_c w_s \cosh\left(\frac{\mathbf{q}\mathbf{u}_s}{T_s}\right) \cos(2q x_s)}{w_c^2 e^{\frac{2\mathbf{k}\mathbf{u}_s}{T_s}} + w_s^2 e^{-\frac{2\mathbf{k}\mathbf{u}_s}{T_s}} + 2w_c w_s} . \quad (26)$$

Note that this result is valid for the case when $\hat{\mathbf{k}}$ points to the $+x$ direction, because the weights depend on this and $w_c > w_s$. See Fig. 7. The fact that the emission from the source, which is closer to the detector is stronger makes the direction of the flow detectable.

If we introduce the notation $w_c = 1 + \epsilon$ and $w_s = 1 - \epsilon$, the deviation from the symmetric result will become apparent

$$C(k, q) \Big|_{+x} = 1 + \exp(-R^2 q^2) \times \frac{(1 + \epsilon^2) \cosh\left(\frac{2\mathbf{k}\mathbf{u}_s}{T_s}\right) + 2\epsilon \sinh\left(\frac{2\mathbf{k}\mathbf{u}_s}{T_s}\right) + (1 - \epsilon^2) \cosh\left(\frac{\mathbf{q}\mathbf{u}_s}{T_s}\right) \cos(2q x_s)}{(1 + \epsilon^2) \cosh\left(\frac{2\mathbf{k}\mathbf{u}_s}{T_s}\right) + 2\epsilon \sinh\left(\frac{2\mathbf{k}\mathbf{u}_s}{T_s}\right) + (1 - \epsilon^2)} . \quad (27)$$

If $\epsilon \rightarrow 0$, i.e. if $w_c = w_s$, we recover the earlier result, Eq. (21). If $\epsilon = 0$ we have the symmetric situation where both sources have equal contribution, the asymmetric terms vanish, and the result becomes to be symmetric for the change of the direction of the flow velocity. This result has terms, which change sign if the flow velocity, \mathbf{u}_s changes sign. The result is valid only if the detector is in the $\hat{\mathbf{k}} = (1, 0, 0)$ direction. For this direction, however, if the flow velocity points in the z -direction, i.e. orthogonal to \mathbf{k} the asymmetric term does not provide any contribution, so it

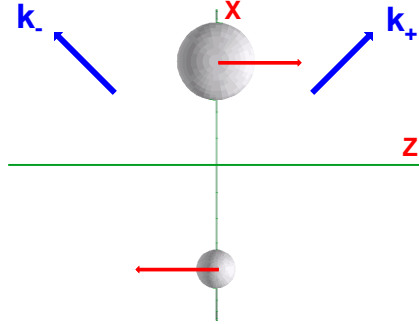


Fig. 8. (color online) Two moving sources in the reaction ($[x-z]$) plane, separated in the x -direction. The sources are moving in the directions indicated by the (red) arrows. The two "tilted" detector directions are indicated by the (blue) arrows labeled with k_+ and k_- .

will not show up in $C(k_x, \mathbf{q})$. To circumvent this problem we should study detector directions, which do not coincide with the primary axes of the given event (where x is the direction of the impact parameter vector, \mathbf{b} , pointing to the projectile; y is the other transverse direction; and z is the direction of the projectile beam).

Correlation in Tilted Directions: The form of the correlation function is the same if \mathbf{k} is in the same plane, the reaction plane, but it has a z component also, i.e. $\mathbf{k} = (k_x, 0, \pm k_z)$. This is possible for all LHC heavy ion experiments, ATLAS, CMS and even ALICE, where the longitudinal acceptance range of the TPC ($\Delta\eta < 0.8$) is the smallest. See Fig. 8.

Depending on the detector acceptance we should choose a detector direction where $|k_z|$ is as big as the detector acceptance allows it. For this configuration the **form** of the correlation function is the same as (27)

$$C(k, q) \Big|_{+x, \pm z} = C(k, q) \Big|_{+x}, \quad (28)$$

with keeping the different weights, w_c, w_s or ϵ so that the forward shifted and backward shifted directions have the same weights. These weights are not specified up to now.

For detection of the correlation function we have to introduce here the usual, \mathbf{k} -dependent coordinate system to classify the direction of \mathbf{q} . Thus if

$$\hat{\mathbf{k}}_{\pm} = (a, 0, \pm b) \text{fm}^{-1}, \quad k_x = a|\mathbf{k}|, \quad k_z = \pm b|\mathbf{k}|, \quad (29)$$

where $a^2 + b^2 = 1$, see Fig. 8, then the difference vector, \mathbf{q} , can be measured in the directions

$$\begin{aligned} \hat{\mathbf{q}}_{out} &= (a, 0, \pm b), \quad q_x = a|\mathbf{q}|, \quad q_z = \pm b|\mathbf{q}| \\ \hat{\mathbf{q}}_{side} &= (0, 1, 0), \quad q_y = |\mathbf{q}| \\ \hat{\mathbf{q}}_{long} &= (\mp b, 0, a), \quad q_x = \mp b|\mathbf{q}|, \quad q_z = a|\mathbf{q}|. \end{aligned} \quad (30)$$

This leads to the following correlation functions

$$\begin{aligned}
 C(k_{(\pm)}, q_{out}) &= 1 + \exp(-R^2 q^2) \times \\
 &\frac{(1+\epsilon^2) \cosh\left(\frac{2\gamma k_z v_z}{T_s}\right) + 2\epsilon \sinh\left(\frac{2\gamma k_z v_z}{T_s}\right) + (1-\epsilon^2) \cosh\left(\frac{\gamma q_z v_z}{T_s}\right) \cos(q_x d_x)}{(1+\epsilon^2) \cosh\left(\frac{2\gamma k_z v_z}{T_s}\right) + 2\epsilon \sinh\left(\frac{2\gamma k_z v_z}{T_s}\right) + (1-\epsilon^2)}, \\
 C(k_{(\pm)}, q_{side}) &= 1 + \exp(-R^2 q^2), \\
 C(k_{(\pm)}, q_{long}) &= 1 + \exp(-R^2 q^2) \times \\
 &\frac{(1+\epsilon^2) \cosh\left(\frac{2\gamma k_z v_z}{T_s}\right) + 2\epsilon \sinh\left(\frac{2\gamma k_z v_z}{T_s}\right) + (1-\epsilon^2) \cosh\left(\frac{\gamma q_z v_z}{T_s}\right) \cos(q_x d_x)}{(1+\epsilon^2) \cosh\left(\frac{2\gamma k_z v_z}{T_s}\right) + 2\epsilon \sinh\left(\frac{2\gamma k_z v_z}{T_s}\right) + (1-\epsilon^2)}.
 \end{aligned} \tag{31}$$

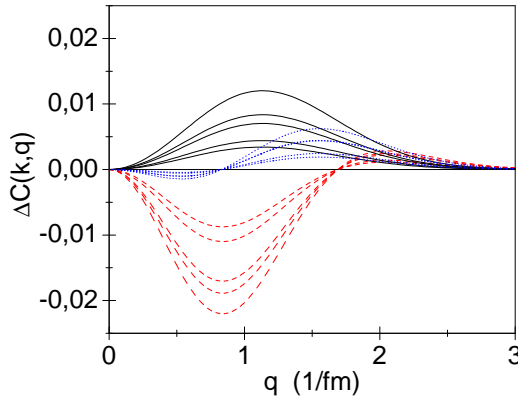


Fig. 9. (color online) Difference of the forward and backward shifted correlation function, $\Delta C(k_{\pm}, q_{out})$, for the value $\epsilon = 0.50$. The *solid black lines* are for the velocity $v_z = 0.5c$, *dotted blue lines* are for the velocity $v_z = 0.6c$ and *dashed red lines* are for the velocity $v_z = 0.7c$. Displacement is $d_x = 1.0$ fm, $T_s = 0.139$ GeV and $a = b = 1/\sqrt{2}$. The values of k are: for the *solid black lines* 0.25, 0.50, 2.00, 2.75 and 3.50 fm^{-1} , the *dotted blue lines* 0.25, 0.50, 1.00, 1.75 and 2.50 fm^{-1} , and the *dashed red lines* 0.25, 0.50, 0.75, 1.25 and 1.75 fm^{-1} .

Although, it seems that $C(k_{(\pm)}, q_{out})$ and $C(k_{(\pm)}, q_{long})$ are the same, this is in fact not the case, because the values of the components of the different types of \mathbf{k} and \mathbf{q} are not the same as described in Eqs. (29,30). In all cases, the out-, side- and long- $q = |\mathbf{q}|$. We will also use the notation $k = |\mathbf{k}|$ and $\gamma v_x = u_x$, $\gamma v_y = u_y$, $\gamma v_z = u_z$, so that $\mathbf{u}_s = (u_x, u_y, u_z)$. For example for the *out* component the difference of the forward and backward shifted correlation functions is

$$\begin{aligned}
 \Delta C(k_{\pm}, q_{out}) &\equiv C(k_+, q_{out}) - C(k_-, q_{out}) = \\
 &\frac{4 \exp(-R^2 q^2) \epsilon \sinh\left(\frac{2u_z b k}{T_s}\right) (1-\epsilon^2) \left[1 - \cosh\left(\frac{u_z b q}{T_s}\right) \cos(a q d_x)\right]}{\left[(1+\epsilon^2) \cosh\left(\frac{2u_z b k}{T_s}\right) + (1-\epsilon^2)\right]^2 - 4\epsilon^2 \sinh^2\left(\frac{2u_z b k}{T_s}\right)}.
 \end{aligned} \tag{32}$$

As Eq. (32) and Fig. 9 show, the Differential Correlation Function (DCF), $\Delta C(k_{\pm}, q_{out})$, is sensitive to the speed and direction of the rotation, and it is also sensitive to the amount of the tilt in the directions of the detection, regulated here by the parameters a and b . $\Delta C(k_{\pm}, q_{out})$ tends to zero both if $q \rightarrow 0$ and if $q \rightarrow \infty$. In case if the detector has a narrow pseudorapidity acceptance, then \mathbf{k}_{\pm} is close to

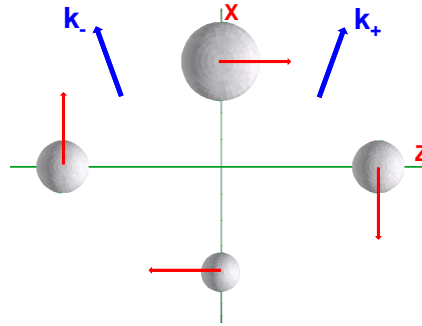


Fig. 10. (color online) Four moving sources in the reaction ($[x - z]$) plane, separated in the x - and z - directions. The sources are moving in the directions indicated by the (red) arrows. The "tilted" detector directions are indicated by the (blue) arrows.

k_x , i.e. $b \ll a$ and then the weights are maximal for the source in the x -direction.

The $\sinh(2u_z bk/T_s)$ term in eq. (32) changes sign in the nominator when u_z changes sign the difference of the two correlation functions, $\Delta C(k_{\pm}, q_{out})$ changes sign also because all other terms are symmetric to the sign change of the velocity.

This is an important observation as we can detect the direction and magnitude of the rotation in the reaction plane. This difference is also increasing with the longitudinal shift, b , of the average momentum vector, \mathbf{k} , so that detectors with larger pseudorapidity acceptance can detect the rotation better.

In order to perform this measurement, one has to determine the global reaction plane (e.g. from spectator residues in the ZDCs), and determine the projectile side of this plane as it was mentioned earlier. Furthermore the event by event center of mass should also be identified (using e.g. the method shown in Ref. 22, 23). This will be the positive x -direction. Then the correlation function can be measured for four different \mathbf{k} -directions in the global reaction plane. These four directions are shifted forward and backward from the center of mass symmetrically on the projectile side, and there should be a symmetric pair of detection points in the target side of the reaction plane too. In the realistic case with taking into account asymmetries that arise from the freeze out, the proper determination of the c.m. and reaction plane are even more important.

The \mathbf{k} directions opposite to each other across the c.m. point give the same result, while the difference, $\Delta C(k_{\pm}, q_{out})$, between the Forward (F) and Backward (B) shifted contributions will characterize the speed and direction of the rotation.

This symmetry can be used to eliminate the contribution from eventual random fluctuations. The observed F/B asymmetry depends on the parameters ϵ , v_z and d_x , these can be estimated by measuring the correlation functions at all possible moments \mathbf{k} .

2.3. Emission from four sources

With four sources we can illustrate the possibilities of differential HBT method studies in different directions. The correlation functions can be calculated in general for four sources and two detector positions. This can then be applied to different detector configurations.

The out component of the four source correlation function with weight factors $\omega_a, \omega_b, \omega_c, \omega_d$ can be found by using the same method as for the two source case. Two examples on different detector configurations are given in Figs. 10 and 11. We

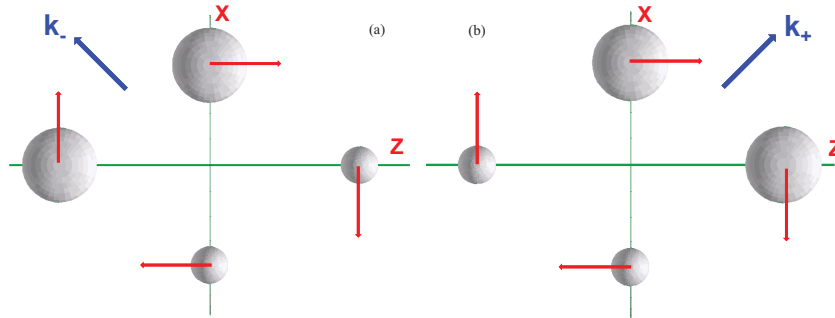


Fig. 11. (color online) Four moving sources in the reaction ($[x - z]$) plane, separated in the x - and z - directions. The sources are moving in the directions indicated by the (red) arrows. The "tilted" detector directions are indicated by the (blue) arrows. In the two configurations, (a) and (b) the detector directions are different and the weights of the sources are also different, so that the sources closer to the detector direction have larger weights.

use the same equations as in the two source model, Eqs. (29) and (30). A source with a larger weight factor is closer to the detector, so that $\omega_a, \omega_b, \omega_c, \omega_d$ correspond to $\mathbf{x}_s \equiv (r_x, r_z) = (d_x, 0), (-d_x, 0), (0, d_z), (0, -d_z)$ respectively.

In case if the detector has a wide pseudorapidity acceptance, then \mathbf{k}_\pm can deviate significantly from k_x , i.e. $b \geq a$ and then the weights are maximal for the two sources closest to \mathbf{k}_+ or \mathbf{k}_- as indicated in Fig. 11. For four sources we can use similar approach to find the difference of the forward and backward correlation functions. We will use that $d_x = d_z, v_x = v_z$ and $a = b$.

Some examples for the differential correlation functions are shown in Figs. 12. Here due to the simplified few source model we specified the weight distribution among the sources in a simplified way. For realistic high resolution fluid dynamical model calculations the realistic evaluation of emission probabilities is performed in Ref. 21. We can compare Fig. 12 (Left) with the previously shown two source model,

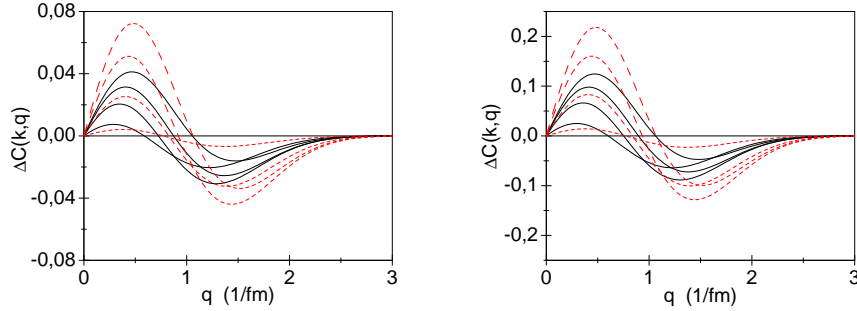


Fig. 12. (color online) **Left:** The Differential Correlation Function for the weight factors: $\omega_a = 1.25$, $\omega_b = 0.75$, $\omega_c = \omega_d = 1.00$ for sources placed at $+x$, $-x$, $+z$ and $-z$ respectively. This weight distribution corresponds to the configuration shown in Fig. 10. The *solid black lines* are for the velocity $v_z = 0.5c$, and the *dashed red lines* are for the velocity $v_z = 0.7c$. Displacement is $d_x = d_z = 1.0$ fm, $T_s = 0.139$ GeV and $a = b = 1/\sqrt{2}$. The values of k are: for the *solid black lines* 0.10, 0.50, 1.00, and 2.00 fm^{-1} and for the *dashed red lines* 0.10, 0.50, 1.00, and 2.00 fm^{-1} . The difference is larger for smaller values of k . **Right:** The Differential Correlation Function for the weight factors: $\omega_a = 1.25$, $\omega_b = 0.75$, $\omega_c = 1.50$, $\omega_d = 0.50$ for sources placed at $+x$, $-x$, $+z$ and $-z$ respectively (Fig. 11b) and $\omega_a = 1.25$, $\omega_b = 0.75$, $\omega_c = 0.50$, $\omega_d = 1.50$ for sources placed at $+x$, $-x$, $+z$ and $-z$ respectively (Fig. 11a). All other parameters are the same as in the left figure. The shape is similar to the figure on the left, however the amplitude is different. The larger amplitude arises from the enhanced weight factor for those sources which are closer to the average emission directions \mathbf{k}_- , \mathbf{k}_+ in the Differential Correlation Function.

Fig. 9, and we see that the amplitudes are similar but the shapes are different. First of all the sensitivity on the direction of rotation remained the same as in the simpler two source model. The two extra sources, c and d lead to higher amplitude for the Differential Correlation Function, while the regular positions of the locations of the zero points are varying due to more sources with different weight parameters.

If the detector acceptance is wider, then the two detectors can be placed at more different angles. This configuration makes the forward and backward placed sources more accessible to the forward and backward detectors, respectively. This is taken into account in the emission weights of our sources. These weights are now different for the two components of the DCF! The result shows the tendency that the DCF has a similar structure in the two source model and the four source model in a resembling configuration. Fig. 12 (Right) has the same shape as Fig. 12 (Left), but the amplitude is larger.

3. Conclusions

In this work we study the possibility of detecting and evaluating the rotation of a source by the specific use of the Hanbury-Brown and Twiss method for rotating systems. Our primary interest was the application for peripheral ultra-relativistic heavy ions collisions with large angular momentum. In the above demonstrated examples the angular momentum per nucleon is given by $\mathbf{L}_N = (1/s) \sum_{i=1}^s \mathbf{d}_i \times \mathbf{p}_i$

$= (\gamma m_N / s) \sum_{i=1}^s \mathbf{d}_i \times \mathbf{v}_i$, where s is the number of sources. In the examples \mathbf{L}_N can easily be obtained as \mathbf{d}_s and \mathbf{v}_s were always orthogonal to each other.

It turned out that it is important to take into account that the particles reaching the detector cannot reach it with equal probability from the near side and the far side of the emitting object. With this fact considered we could obtain correlation functions, which reflect the properties and also the direction of the flow.

We studied the Differential Hanbury Brown and Twiss method, which made it possible to trace down the rotation in relativistic heavy ion collisions by measuring the correlation functions in the reaction plane at nearly transverse angles to the beam direction. The method is promising and can be performed in most heavy ion experiments without difficulties, as well as it can be implemented in different reaction models, like fluid dynamical models, microscopic transport models and hybrid models. In full scale theoretical models, the emission probabilities from the FO layer have been studied earlier.²¹ In this case we applied the method to a high resolution, 3+1D, computational fluid dynamics model, which was used earlier to predict rotation, KHI, flow vorticity, and polarization.^{1, 2, 4, 20}

In our simple analytic models we could show that if we change the direction of rotation to the opposite the Differential Correlation Function changes sign due to the sinh function in the nominator. In this configuration with the change of the tilt of the detector directions we can adjust the DCF, to the threshold value where the $\Delta C(k_{\pm}, q_{out})$, is still positive, which provides a sensitive estimate for the rotation velocity at Freeze Out.

These analytic results provide deeper insight to the methods of studying rotation in highly energetic systems. Several aspects of the sensitivity and observability can be discussed based on these analytic results which are not easily accessible in a fully realistic and complex reaction model.

Acknowledgements

Enlightening discussions with Marcus Bleicher, Tamás Csörgő, Dariusz Miskowiec, Horst Stöcker, Dujuan Wang, and scientists of the Frankfurt Institute for Advanced Studies are gratefully acknowledged.

References

1. L.P. Csernai, V.K. Magas, H. Stöcker, and D.D. Strottman, Phys. Rev. C **84**, 024914 (2011).
2. L.P. Csernai, D.D. Strottman and Cs. Anderlik, Phys. Rev. C **85**, 054901 (2012).
3. D.J. Wang, Z. Nédá, and L.P. Csernai Phys. Rev. C **87**, 024908 (2013).
4. L.P. Csernai, V.K. Magas, and D.J. Wang, Phys. Rev. C **87**, 034906 (2013).
5. S. Floerchinger and U. A. Wiedemann, Journal of High Energy Physics, JHEP **11**, 100 (2011).
6. S. Floerchinger and U. A. Wiedemann, J. Phys. G: Nucl. Part. Phys. **38**, 124171 (2011).
7. R. Hanbury Brown and R.Q. Twiss, Phil. Mag. **45**, 663 (1954).
8. R. Hanbury Brown and R.Q. Twiss, Nature, **178**, 1046 (1956).

9. G. Goldhaber, S. Goldhaber, W. Lee and A. Pais, Phys. Rev. **120**, 300 (1960).
10. D. Miskowiec, and E877 Collaboration, Nucl. Phys. A **590**, 557c (1995).
11. M.A. Lisa, N.N. Ajitanand, J.M. Alexander, et al., Phys. Lett. B **496**, 1 (2000).
12. M.A. Lisa, U. Heinz, U.A. Wiedemann, Phys. Lett. B **489**, 287 (2000).
13. E. Mount, G. Graef, M. Mitrovski, M. Bleicher, M.A. Lisa, Phys. Rev. C **84**, 014908 (2011).
14. S. Pratt, Phys. Rev. D **33**, 1314 (1986).
15. Yu.M. Sinyukov, Nucl. Phys. A **498**, 151c (1989).
16. Qingfeng Li, J. Steinheimer, H. Petersen, M. Bleicher, H. Stöcker, Phys. Lett. B **674**, 111 (2009).
17. Qingfeng Li, M. Bleicher, H. Stöcker, Phys. Lett. B **659** 525 (2008).
18. Qingfeng Li, M. Bleicher, Xianglei Zhu, H. Stöcker, J. Phys. G **33** 537 (2007).
19. B. McNnes, arXiv: 1403.3258 [hep-th]
20. F. Becattini, L.P. Csernai, D.J. Wang, Phys. Rev. C **88**, 034905 (2013)
21. L. P. Csernai, S. Velle, and D. J. Wang , Phys. Rev. C **89**, 034916 (2014).
22. L.P. Csernai, G. Eyyubova, V.K. Magas, Phys. Rev. C **86**, 024912 (2012).
23. L.P. Csernai, G. Eyyubova, V.K. Magas, Phys. Rev. C **86**, 019902 (2013).
24. V. Vovchenko, D. Anchishkin, L.P. Csernai, Phys. Rev. C **88**, 014901 (2013).
25. S. Zschocke, Sz. Horvat, I.N. Mishustin, L.P. Csernai Phys. Rev. C **83**, 044903 (2011).
26. F. Jüttner, Ann. Phys. und Chemie, **34** (1911) 856.
27. W. Florkowski: *Phenomenology of Ultra-relativistic heavy-Ion Collisions*, World Scientific Publishing Co., Singapore (2010).
28. A.N. Makhlin, Yu.M. Sinyukov, Z. Phys. C **39**, 69-73 (1988).
29. F. Cooper, G. Frye, Phys. Rev. D **10**, 186 (1974).
30. T. Csörgő, Heavy Ion Phys. **15**, 1-80, (2002).
31. Sz. Horvát, V.K. Magas, D.D. Strottman, L.P. Csernai, Phys. Lett. B **692**, 277 (2010).
32. P.K. Kovtun, D.T. Son and A.O. Starinets, Phys. Rev. Lett. **94**, 111601 (2005).
33. L.P. Csernai, J.I. Kapusta, L.D. McLerran, Phys. Rev. Lett. **97**, 152303-4 (2006).
34. E. Molnár, L. P. Csernai, V. K. Magas, Zs. I. Lazar, A. Nyiri, and K. Tamosiunas, J. Phys. G **34**, 1901 (2007).
35. E. Molnár, L. P. Csernai, V. K. Magas, A. Nyiri, and K. Tamosiunas, Phys. Rev. C **74**, 024907 (2006).
36. E. Molnár, L.P. Csernai, V.K. Magas, Acta Phys. Hung. A **27**, 359 (2006).
37. Yu.M. Sinyukov, Yad. Fiz. **50**, 228 (1989).
38. Yu.M. Sinyukov, Sov. J. Nucl. Phys. **50**, 143 (1989).
39. Yu.M. Sinyukov, Z. Phys. C **43**, 401 (1989).
40. K.A. Bugaev, Nucl. Phys. A **606**, 559 (1996).
41. Cs. Anderlik, Z.I. Lázár, V.K. Magas, L.P. Csernai, H. Stöcker and W. Greiner, Phys. Rev. C **59**, 388 (1999).
42. C. Anderlik, L.P. Csernai, F. Grassi, W. Greiner, Y. Hama, T. Kodama, Z.I. Lázár, V.K. Magas and H. Stöcker, Phys. Rev. C **59**, 3309 (1999) .
43. V.K. Magas, C. Anderlik, L.P. Csernai, F. Grassi, W. Greiner, Y. Hama, T. Kodama, Z.I. Lázár and H. Stöcker, Nucl. Phys. A **661**, 596c (1999).
44. L.P. Csernai, J. Phys. G **28**, 1993 (2002).
45. V.K. Magas, A. Anderlik, Cs. Anderlik and L.P. Csernai, Eur. Phys. J. C **30**, 255 (2003).
46. K. Tamosiunas and L.P. Csernai, Eur. Phys. J. A **20**, 269 (2004).
47. V.K. Magas, L.P. Csernai, E. Molnár, A. Nyiri, K. Tamosiunas, Nucl. Phys. A **749**, 202 (2005).
48. V.K. Magas, L.P. Csernai, E. Molnár, Acta Phys. Hung. A **27**, 351 (2006).